# Electronic Supplementary Information

# Hierarchical self-assembly of miktoarm star copolymers with pathway complexity

Jie Xiao,[a] Qun He,*[a] Minjun Yang,[a] Haoquan Li,[a] Xiandeng Qiu,[a] Binghua Wang,[c] Bin Zhang,[c] and Weifeng Bu*[ab]

[a]Key Laboratory of Nonferrous Metals Chemistry and Resources Utilization of Gansu Province, State Key Laboratory of Applied Organic Chemistry, and College of Chemistry and Chemical Engineering, Lanzhou University, Lanzhou, 730000, China
[b]State Key Laboratory of Solid Lubrication, Lanzhou Institute of Chemical Physics, Chinese Academy of Sciences, Lanzhou 730000, China
[c]School of Materials Science and Engineering, Zhengzhou University, Zhengzhou, 450002, China

**General Considerations.** Polyoxometalate based miktoarm star copolymers (**SEW-1−5**) were respectively synthesized by ionic exchange reactions of a polyoxometalate (POM) cluster of $K_4[\alpha\text{-}SiW_{12}O_{40}]$ and polystyrene-*block*-poly(ethylene glycol) copolymers with a central 1,2,3-triazolium group ($PS_n$-$b^+$-$PEG_mI^-$, $n$ = 17, 26, 39, 57, 81; $m$ = 45) (See the literature: Xiao, J.; He, Q.; Qiu, S.; Li, H.; Wang, B.; Zhang B.; Bu, W. Amphiphilic miktoarm star copolymers can self-assemble into micelle-like aggregates in nonselective solvents: a case study of polyoxometalate based miktoarm stars. *Sci. China Chem.* **2020**, *63*, 792−801). These miktoarm star copolymers cannot be directly dissolved in the methanol based mixture solvents. Therefore, the miktoarm stars were dispersed first in the nonselective solvents of THF, toluene, or chloroform, and then methanol was added with volume ratios from 10 to 90%. The former three solvents are the good solvents of both the $\mathbf{PS}_{\boldsymbol{n}}$ and $\mathbf{PEG}_{\boldsymbol{m}}$ arms ($\boldsymbol{n}$ = 17, 26, 39, 57, 81; $\boldsymbol{m}$ = 45). Whereas, methanol is the poor and good solvents of the $\mathbf{PS}_{\boldsymbol{n}}$ and $\mathbf{PEG}_{\boldsymbol{m}}$ arms, respectively. Their final concentrations in these solvent mixtures were controlled at 0.5 mg/mL. Dynamic light scattering (DLS) was performed on a Malvern Zetasizer instrument at a fixed detection angle of 173°, where the solution concentration was 0.5 mg $mL^{-1}$. TEM images were recorded on an *FEI Talos F200S* with an accelerating voltage 200 kV, where the sample solutions (0.5 mg $mL^{-1}$) were drop-cast onto carbon-coated copper grids or copper grids coated with perforated polymer membranes. Scanning electron microscopy (SEM) measurements were performed on a field emission scanning electron microscope (Hitachi S-4800), before which we deposited a 5-nm thick gold layer on the specimen by using Hitachi E-1045 ion sputter. This coating can prevent efficiently electric charging generated during the process of SEM measurements, leading to high quality SEM images. Static contact angles of water were obtained from by a wetting analysis system of *KRüSS* DSA100, where the sample solutions (0.5 mg $mL^{-1}$) were cast onto glass substrates. Such tests were repeated five times for reproducibility. AFM measurements were carried out using a Dimension Icon microscope from Bruker. All measurements were carried out at room

temperature.

**Packing Parameter Calculations.** Packing parameters of the hierarchical nanostructures formed by the miktoarm stars in those methanol based mixture solvents were calculated by the combination of the microscopic observations with the domain sizes of $[\alpha\text{-}SiW_{12}O_{40}]^{4-}$/**PEG$_{45}$**, **PS$_n$**, or **PS$_n$**/$[\alpha\text{-}SiW_{12}O_{40}]^{4-}$. $V_h$ is the hydrophilic volume per formula, which includes the volumes of $[\alpha\text{-}SiW_{12}O_{40}]^{4-}$ ($V_1 = (4/3)\pi(1.04/2)^3 = 0.59$ nm$^3$) and **PEG$_{45}$** ($V_2 = (M_o/\rho_{bulk}N_A) \times 45 = (44.05$ g/mol/1.125 g/mL $\times$ $6.022\times10^{23}$/mol) $\times$ 45 = 2.93 nm$^3$), where $M_o$, $\rho_{bulk}$, and $N_A$ are the monomer molecular weight, **PEG** density, and Avogadro's constant, respectively. The volumes of the cylindrical ($V_c$) and spherical cores ($V_s$) were calculated, respectively, by $V_c = \pi R^2 l$ and $V_s = 4/3\pi R^3$, where $R$ and $l$ is the radius of the ionic cores and the length of the cylindrical micelles obtained from the TEM images ($R = d/2$). The aggregation numbers ($N_{agg}$) of the micelle were calculated by $N_{agg} = V_c$ or $V_s/V_h$. The interfacial area per chain ($A_c$) is given by $A_c = A_t/N_{agg}$, where $A_t$ is the total area of the core−corona interface. Therefore, the grafting density can be calculated on the basis of the following equation: $\sigma = \sigma_0(r_0/r)$ (cylinders) or $\sigma_0(r_0/r)^2$ (spheres), where $r_0$ and $r$ the core radii of the micelles obtained from the chloroform and chloroform/methanol mixture solvent, respectively.

**Additional Results and Discusssion.**

**Comparable nanofibers of SEW-2 also formed in the THF/methanol mixture solvent with a methanol composition of 90 vol % (Fig. S2 and Table 2).** Moreover, the width of the micellar core, the outer and in-between thicknesses of the **PS$_{26}$** coronas were determined to be 4.8 ± 0.2, 6.5 ± 0.3 and 5.4 ± 0.2 nm, respectively (Table 2). The latter two values were consistent with those found in the nanofibers formed at the methanol content of 50 vol %.

Alternatively, there was a possibility that the interior PS chains could be re-shaped by decreasing their stretching degree, wherein the micelle units were not in the spherical shape but in an ellipse-like shape. As already documented theoretically,[S1] star homopolymers collapse into a compact globule in poor solvents. In two-star or three-star systems, the grafted chains overlap significantly as a result of inter-star van der Waals attractions. Such overlapped grafted chains have been captured by several experimental studies.[S2] Moreover, in the present study, these **PS** tails were comparable to those small-molecule amphiphiles in length. In their self-assembled structures, fully interdigitated alkyl chains were commonly observed.[S3] Therefore, we preferred to the statement that the interior **PS$_{26}$** chains were fully interdigitated.

**Comparable nanofibers of SEW-2 formed in the toluene/methanol mixture solvent with a methanol composition of 90 vol %.** By contrast, upon increasing the methanol content to 90 vol %, **SEW-2** self-assembled into bundled nanofibers (Fig. S3 and Table S5), similar to those found in the THF/methanol mixture solvents (Fig. 2, S2, and Table 2). The corresponding width of the cylindrical core, the outer and in-between thicknesses of the **PS$_{26}$** coronas were estimated to be 4.8 ± 0.4, 6.0 ± 0.2 and 4.2 ± 0.3 nm, respectively. Similar to the above situation from the THF/methanol mixtures, the contractive cylindrical core resulted in an appreciable increase in the grafting density of the **PS$_{26}$** chain, further inducing a highly stretched **PS$_{26}$** chain (Fig. 2, S2, and Table 2). The much shorter thickness of the inner corona (4.2 nm) was consistent with the poorer solvent quality, leading to stronger inter-cylinder van der Waals attractions between the **PS$_{26}$** chains. Therefore, it was reasonable to find a coexistence of free-standing sheets and bundled nanofibers when **SEW-2** was dispersed in the mixture solvent with an intermediate methanol content of 75 vol % (Fig. S4).

**The hierarchical self-assembly processes to form sheetlike assemblies were generalized**

**with increasing the length ratio of $PS_n$ to $PEG_{45}$ ($n$ = 39, 57, 81) in the cases of SEW-3−5.** The self-assembly behaviors of **SEW-2** raised an intriguing question of whether the present approach was universal to fabricate hierarchical nanostructures with multi-level complexity for the miktoarm star copolymers. To clarify this question, we further investigated solution self-assembly processes of **SEW-3−5**, in which the $n$ value of the $PS_n$ arm was increased successively from 39 to 57 to 81, while the $PEG_{45}$ arm remained constant. The miktoarm stars of **SEW-3−5** self-assembled to generate sheetlike assemblies in the toluene/methanol mixture solvent with a methanol content of 50 vol % (0.5 mg/mL, Fig. S5 and S6). The sheets exhibited water contact angles of 104°, 102°, and 106°, respectively, suggestive of highly hydrophobic surfaces. Among these sheets, the dark cylindrical cores of $[\alpha\text{-}SiW_{12}O_{40}]^{4-}$/$PEG_{45}$ were isolated with the gray $PS_n$ coronas ($n$ = 39, 57, 81), where the cylindrical micelles were aligned *via* both side-to-side and end-to-end stacking forms (Fig. S5 and S6). The thicknesses of the cylindrical cores were measured to be 5.6, 4.8, and 4.2 nm in the cases of **SEW-3**, **SEW-4**, and **SEW-5**, respectively, while the widths of the in-between $PS_n$ coronas were 9.5, 10.9, and 13.1 nm (Table S4). The former three values, together with the core thickness of the cylindrical micelle of **SEW-2** (6.0 nm, vide supra), showed that the cylindrical core exhibited a recognizable decrease in thickness with an order of **SEW-2** > **SEW-3** > **SEW-4** > **SEW-5**. Meanwhile, the widths of the in-between coronas increased with increasing the degree of polymerization of the $PS_n$ arms ($n$ = 26, 39, 57, 81, Table S4). The width of the in-between corona of **SEW-3** (9.5 nm) was consistent with the contour length of the $PS_{39}$ chain (0.25 × 39 = 9.75 nm). Once again, this was indicative of the full interpenetration of the $PS_{39}$ chains and thus the inter-cylinder van der Waals attractions, leading to the fabrication of the sheetlike assemblies. Whereas, in the cases of **SEW-4** (10.9 nm) and **SEW-5** (13.1 nm), the widths of the in-between coronas were clearly smaller than the fully extended lengths of the $PS_{57}$ (0.25 × 57 = 14.25 nm) and $PS_{81}$ chains (0.25 × 81 = 20.25 nm, Table S4), respectively. These results suggested that the van der Waals attractive force increased with increasing the molecular weight of the $PS_n$ blocks. This would lead inevitably to the increasing contraction of the $[\alpha\text{-}SiW_{12}O_{40}]^{4-}$/$PEG_{45}$ core, agreeing well with the above decreasing core thickness (Table S4). Finally, the total widths of the cylindrical micelles of **SEW-3−5** in the free-standing sheets were determined to be 15.1, 15.7, and 17.3 nm, respectively (Table S4). Analogous to **SEW-2** (14.3 nm, Fig. 3), these width values were further considered to be the thicknesses of the free-standing sheets (Table S4). In all these cases, the grafting densities of the $PS_n$ chains ($n$ = 26, 39, 57, 81) showed a recognizable increase, consistent with those occurring in the THF/methanol and chloroform/methanol dispersions of **SEW-2** (Table 2 and S4).

As reported previously,[53] cylindrical micelles showed a coexistence with ricelike or spherical micelles in the toluene solutions of **SEW-3** (the number ratio of cylinders: 20%) and **SEW-4** (10%), while **SEW-5** self-assembled to generate a pure spherical micelle phase. However, the ricelike or spherical micelles were no longer visible in the sheetlike assemblies under the present solvent condition (toluene/methanol = 1:1, v/v). These scenarios were consistent with the morphological change from ricelike to cylindrical micelles occurring in the case of **SEW-2** under the same solvent condition (Fig. 3). To further unveil the self-assembly process and mechanism, **SEW-5** was chosen as a typical miktoarm star because of its pure spherical micelle phase in toluene.[53] Upon decreasing the methanol composition to 10 vol %, representative BF-TEM images displayed that spherical micelles coexisted with cylindrical micelles (Fig. S7a−c). The dark cores of the sphere and cylinder were 5.6 and 4.8 nm, respectively. Their middle spacings were assigned to the $PS_{81}$ chains and the domain width was 14.5 nm. The lengths of the cylinders were in the micrometric range and a

cylinder with a length of ca. 2.0 μm was clearly observed (Fig. S7b). However, the cylindrical micelle occupied a number ratio of only 5%. Further increasing the methanol volume ratio to 25% caused similar coexistence of spheres with micrometric length cylinders (Fig. S7d−f). The number ratio of the cylindrical micelle was estimated to be ca. 30%. These increasing number ratios indicated that sphere-to-cylinder transition states were arrested clearly under these two solvent conditions. Finally, when **SEW-5** was dispersed in the toluene/methanol mixture solvent with a methanol content of 50 vol %, the spherical micelles were completely transformed to yield cylindrical micelles (Fig. 4 and 1c). The cylindrical micelles further self-assembled *in situ* into the free-standing sheets as a result of inter-cylinder van der Waals attractions between the $\mathbf{PS}_{n}$ coronas (Fig. S5−S7). With increasing the methanol content in toluene, the $\mathbf{PEG_{45}}$ arm became progressively more solvated together with the partially desolvated $\mathbf{PS}_{n}$ blocks. This would lead to an appreciable increase in the relative volume of the $[\alpha\text{-}SiW_{12}O_{40}]^{4-}$/$\mathbf{PEG_{45}}$ interiors in these toluene/methanol mixture solvents. Meanwhile, the weakened solvent quality (50 vol % methanol) for the $\mathbf{PS}_{n}$ arms resulted in the shortened cylinders (150 ~ 550 nm), as compared to the above micrometric cylinders in the cases of 10 vol % and 25 vol % methanol contents (Fig. S5−S7). Such a hierarchical self-assembly process was not observed in the THF/methanol or chloroform/methanol mixture solvents, as documented later (vide infra). Once again, this should be due to the unique van der Waals interaction of the toluene molecules with the $\mathbf{PS}_{n}$ blocks under the present solvent conditions.

**SEW-2 self-assembled to form bundlelike nanofibers coexisting with multi-micelle aggregates on dispersion in the chloroform/methanol mixture solvents with methanol volume ratios of 50% and 90%.** The packing parameters of the nanofibers were almost consistent with those found in the THF/methanol mixture solvents (Fig. S8 and Table S5). The outer gray corona of the multi-micelle aggregate occupied an average thickness of 6.0 nm and was assigned to the $\mathbf{PS_{26}}$ chains (Fig. S8c and f). Further scrutiny of the central part revealed that it was composed of dark nanospheres isolated with gray nanodomains. The dark nanosphere possessed a mean diameter of 6.5 nm and were accordingly attributed to the $[\alpha\text{-}SiW_{12}O_{40}]^{4-}$/$\mathbf{PEG_{45}}$ core. The in-between spacing was averaged to be about 4.8 nm, which was slightly smaller than the corona thickness (6.0 nm). Again, the coronal $\mathbf{PS_{26}}$ chains were highly stretched in both the nanofibers and multi-micelle aggregates, and the $\mathbf{PS_{26}}$ chains between the $[\alpha\text{-}SiW_{12}O_{40}]^{4-}$/$\mathbf{PEG_{45}}$ cores were fully interpenetrated. The diameter of the nanospheres (6.5 nm) was slightly larger than the thickness of the cylindrical core (4.8 nm), which was consistent with the morphological transformation from cylindrical to spherical.[17,18] Correspondingly, the grafting density of the $\mathbf{PS_{26}}$ chain decreased from 0.68 to 0.35 chains/nm$^2$ (Table S5). This picture suggested that some of the cylindrical micelles originally formed in chloroform were broken to yield spherical micelles in the present solvent mixtures, and moreover, the resulting spherical micelles self-assembled *in situ* into multi-micelle aggregates (Fig. S8). The construction of such solid nanostructures was due to the van der Waals attractions between the $\mathbf{PS_{26}}$ chains of the spherical micelles under the present solvent condition, as demonstrated by the fully interpenetrated $\mathbf{PS_{26}}$ chains. Notably, the fracture of cylinder to sphere into the multi-micelle aggregates occurred only in the chloroform/methanol mixture solvents. This was presumably due to the smallest difference of solubility between the $\mathbf{PS_{26}}$ and $\mathbf{PEG_{45}}$ arms in chloroform, as addressed by the solubility parameters (Table S1−S3). Occasionally, vesiclelike aggregates were observed in the methanol content of 90 vol % (Fig. S8f). This would be further rationalized later in the cases of **SEW-3−5**.

**Similarly, SEW-3 also self-assembled into hollow nanostructures (ca. 130 nm) in the**

**toluene/methanol mixture solvent with a methanol percentage of 75 vol %, as demonstrated in both BF-TEM (Fig. 4g and h) and SEM images (Fig. 4i).** The diameter of the [α-$SiW_{12}O_{40}$]$^{4-}$/**$PEG_{45}$** core, the thicknesses of the outside and inside **$PS_{39}$** coronas were 4.7, 7.5 and 6.5 nm, respectively (Table S6). The latter two values showed that the **$PS_{39}$** chains were fully interpenetrated between the spherical micelles of **SEW-3** in the hollow aggregates, as a typical result of inter-micelle van der Waals attractive forces. The total wall thickness of the hollow nanostructures was (7.5 × 2 + 4.7 = 19.7 nm, Table S6). This value was consistent with the naked wall thickness obtained from SEM imaging (29.4 – 10 = 19.4 nm, Fig. 4i). Moreover, the thicknesses of both the outside and inside coronas were much smaller than the contour length of the **$PS_{39}$** chain (9.75 nm), indicative of the occurrence of intra-micelle van der Waals attractions. Moreover, the hollow spheres were connected together to form networks (Fig. 4 and S9). This picture was due to the van der Waals attractions emerging between the hollow spheres, as demonstrated by full contacting or interpenetrating of the outside coronas (Fig. 4). This further resulted in the colloidally instability of the miktoarm star copolymers in the solutions.

The micelle units were presumptively considered with hexagonal closest packing onto the hollow surfaces. Accordingly, the average areas of the single micelle units were determined to be 109 and 200 $nm^2$ for **SEW-3** and **SEW-5**, respectively. Combining the diameters of both the hollow nanostructures and single micelle units, the diameters of the hollow spheres were evaluated to be 111 and 135 nm, further leading to the spherical surface areas of 38 712 and 57 263 $nm^2$, respectively (Table S6). Therefore, the aggregation numbers of the hollow nanostructures were estimated to be (355 and 286) and (1598 and 2860) with regard to the micelle units and miktoarm stars, respectively (Table S6).

**Similar to SEW-4, SEW-5 also formed regular vesicles with a wall thickness of 16.9 nm in the chloroform/methanol mixture solvents with methanol contents with 50 vol % (Fig. S11a and b) and 90 vol % (Fig. S11c and Table S7).** However, in the case of **SEW-3**, the pure phase of vesicular aggregates was formed only at a methanol content of 90 vol % (Fig. S12e and f). The corresponding wall thickness was 13.3 nm. After removing the [α-$SiW_{12}O_{40}$]$^{4-}$ clusters on both sides, the increasing wall thicknesses (11.2, 12.7, and 14.8 nm) in the vesicles of **SEW-3**, **SEW-4**, and **SEW-5** were in good agreement with increasing the molecular weights of the **$PS_n$** arms ($n$ = 39, 57, 81, Table S4). This resulted in an increase in the interfacial area per chain for the **$PS_n$** arms. In the case of **SEW-3**, the decreasing the methanol contents to 25 vol % (Fig. S12a and b), 50 vol % (Fig. S12c), and 75 vol % (Fig. S12d) led to coexistence of regular vesicles with solid multi-micelle aggregates. The wall thicknesses of the vesicles and the diameters of the dark cores in the solid aggregates were estimated to be 12.8 and 6.3 nm, respectively, which were consistent with those above values. These results suggested that both cylindrical and spherical micelles of **SEW-3** formed in chloroform[53] were evolving into regular vesicles in the chloroform/methanol mixture solvents with methanol percentages of 25 ~ 75 vol %. However, such vesicular and intermediate states were caught in the case of **SEW-2** only occasionally with a methanol content of 90 vol % (vide supra, Fig. S8f).

To clarify this self-assembly evolution and mechanism, **SEW-4** was further dispersed in the chloroform/methanol mixture solvents with methanol compositions of 10 vol % and 25 vol %. In the former BF-TEM images, vesicular aggregates coexisted with multi-micelle aggregates (Fig. 6a−d). The wall thickness of the vesicles was consistent with that obtained from the chloroform/methanol mixture solvent (14.8 nm, v/v = 1/1). In the solid spheres, the dark cores of

[α-$SiW_{12}O_{40}$]$^{4-}$/**PEG$_{45}$** were clearly observed with a diameter of 6.3 nm. This value was consistent with the diameter of the spherical micelle (5.9 nm) and the thickness of the cylindrical micelle (6.2 nm) formed by **SEW-4** in chloroform.[53]

Altogether, with increasing the molecular weight of the **PS$_n$** arms ($n$ = 26, 39, 57, 81), the original cylindrical, ricelike, or spherical micelles formed by **SEW-2**−**5** in chloroform[53] exhibited an increasing trend of molecular reorganizations to create regular vesicles in the chloroform/methanol mixture solvents. This was counter-intuitive because the bigger molecular weight was, the harder molecular reorganization would lead to. As well documented before, in micellelike aggregates, the interface area per chain ($A_0$) between the core and corona showed an increasing trend of $A_0$(vesicle) < $A_0$(worm) < $A_0$(sphere).[17,18] For the chloroform solutions of **SEW-2**−**5**, the micellar structures evolved gradually from cylindrical to spherical with a **PS$_n$** corona and a [α-$SiW_{12}O_{40}$]$^{4-}$/**PEG** core.[53] Therefore, the core−corona interface of the micelle in chloroform was expected to be looser and looser. Meanwhile, in such a nonselective solvent, the micellar aggregates coexisted with the unimers of **SEW-5**, as detailed previously.[53] Moreover, in term of the solvent quality for both **PS** and **PEG** arms, the difference of the solubility parameters was in the order of chloroform < THF < toluene. Collectively, it was reasonable that the miktoarm star copolymers preferred to form regular vesicles in the chloroform/methanol mixture solvents with an increasing order of **SEW-2** < **SEW-3** < **SEW-4** < **SEW-5**. This order was slightly different from that in the case of the toluene/methanol mixture solvents (**SEW-2** ≈ **SEW-5** < **SEW-3** < **SEW-4**, Fig. S5−S12), due to the different solvent molecules employed (chloroform versus toluene). It should be highlighted that all of these regular vesicular aggregates differed completely from those hollow structures formed in the toluene/methanol mixture solvents (vide supra, Fig. 4 and S9), but actually belonged to the self-assembly classification of amphiphilic macromolecules in selective solvents.[1−51]

**The unilamellar hollow nanostructures coexisted with bilayered vesicles when SEW-3 was dispersed in the toluene/methanol mixture solvent with a methanol content of 90 vol % (Fig. S13).** Similar intermediate states were also arrested in the case of **SEW-4 (**toluene/methanol = 1/3, Fig. S14**)**. Further increasing the methanol percentage to 90 vol % led to the fabrication of a pure vesicle phase in the case of **SEW-4** (Fig. S15). These bilayered vesicles occupied **PS$_n$** cores ($n$ = 39, 57) and [α-$SiW_{12}O_{40}$]$^{4-}$/**PEG$_{45}$** coronas. This would be discussed in more details later. The formation of the bilayered vesicles were typically due to the molecular reorganizations of **SEW-3** (toluene/methanol = 1/9) and **SEW-4** (toluene/methanol = 1/3 or 1/9) in these selective solvents for the [α-$SiW_{12}O_{40}$]$^{4-}$/**PEG$_{45}$** block. Such molecular reorganizations did not appear in the cases of **SEW-2**, **SEW-3 (**toluene/methanol = 1/3), and **SEW-5**. The former two cases were likely due to the steric hindrance of both the cylindrical and ricelike micelles originally formed by **SEW-2** and **SEW-3** in toluene.[53] Whereas, the latter was presumably assigned to the larger molecular weight of the **PS$_{81}$** arm leading to the really difficult reorganization of **SEW-5** in the corresponding spherical micelles (vide infra).

**Of difference was that SEW-3−5 self-assembled into multi-micelle aggregates in the THF/methanol mixture solvents (Fig. S16−S18).** Among the aggregates of **SEW-3** and **SEW-4**, cylindrical or rodlike micelles coexisted with spherical micelles (Fig. S16 and S17). This was consistent with the reported coexistence of cylinders and rices or spheres emerging in THF.[53] At the methanol content of 90 vol %, the number ratios of the cylinders or rods were reduced significantly in the multi-micelle aggregates (Fig. S16 and S17). This was suggestive of cylinder-to-sphere

transitions under this highly weakened solvent quality for the **PS*n*** coronas ($n$ = 39, 57), consistent with the aforementioned partial cylinder-to-sphere fracture of **SEW-2** dispersed in the chloroform/methanol mixture solvents (Fig. S5). However, these results were completely opposite to those sphere or rice-to-cylinder transformation trends occurring in the toluene/methanol mixture solvents (Fig. 3 and S5−S7). And also, these solid multi-micelle aggregates were in sharp contrast to those hollow nanostructures fabricated in the toluene/methanol mixture solvents (Fig. 4 and S9). The morphological differences presented here were again due to the unique directional interactions between the toluene molecules and the **PS*n*** coronas. Occasionally, normal vesicles were captured only in the case of **SEW-4** (THF/methanol = 1/9, Fig. S17d and e). Moreover, no such bilayered vesicles were observed in both **SEW-3** and **SEW-5** (Fig. S16 and S18), agreeing well with the easier reorganizations of **SEW-4** in the selective solvents, as discussed above.

**The colloidally stable dispersions of SEW-3−5 (chloroform/methanol = 1/9) were further subjected to dynamic light scattering (DLS) measurements.** The resulting DLS plots were indicative of the presence of two diffusive modes (Fig. S19a). The small peaks occupied average hydrodynamic diameters ($D_h$s) of 166, 204, and 190 nm for **SEW-3**, **SEW-4** and **SEW-5**, respectively, corresponding to single regular vesicles. The second DLS signals were even larger than 2 μm, due to the larger aggregates formed by the regular vesicles under the solvent conditions. As addressed previously, both **PEG**-containing block and miktoarm stars can self-associate to generate (micellelike) aggregates in the nonselective solvents of THF or chloroform.[53,S4−S6] Consequently, considering the 10 vol % chloroform in the dispersions of **SEW-3−5**, the formation of such micrometric aggregates was reasonable.

**SEW-1 Self-Assemblied to Generate Nano-Sized Lamellae in These Methanol Based Mixture Solvents.** As reported, self-assembly of **SEW-1** in toluene, THF, and chloroform brought about the formation of nano-sized bilayered structures.[53] They held a **PS$_{17}$** core and [α-$SiW_{12}O_{40}]^{4-}$/**PEG$_{45}$** corona. Typically, methanol was a poor solvent of the **PS$_{17}$** arm and a good solvent of the **PEG** arm, respectively. Upon the addition of methanol (90 vol %) to the toluene, THF, or chloroform solutions of **SEW-1**, the resulting dispersions showed good colloidal stability, in which no precipitates were observed at least for 15 days. Representive TEM images illustrated that **SEW-1** self-assembled in these methanol based mixture solvents to create nano-sized lamellae with planar sizes ranging from 50 to 120 nm (Fig. S20a and b for toluene/methanol, Fig. S20a and b for THF/methanol, and Fig. S20c and d for chloroform/methanol). The edge-on lamellae were clearly observed in the case of chloroform/methanol (Fig. S20c and d), which allowed us to determine the core thickness of **PS$_{17}$**/[α-$SiW_{12}O_{40}]^{4-}$ (4.7 nm, vide infra). After removing the [α-$SiW_{12}O_{40}]^{4-}$ clusters on both the sides of the lamellae, the thickness of the **PS$_{17}$** core was calculated to be 2.6 nm (Table S7). Further, the water contact angles of the corresponding casting films were determined to be 67°, 66°, and 61°, respectively. These values were in accordance with those water contact angles of **PEG**-coated films.[56,57] Consequently, these nano-sized lamellae had a **PS$_{17}$** core and [α-$SiW_{12}O_{40}]^{4-}$/**PEG$_{45}$** corona. This was different from those hierarchical self-assembly behaviors of **SEW-2−5** under the same solvent conditions.

Moreover, as shown in the resulting DLS plots (Fig. S19b), $D_h$s appeared at 456, (1023 and 5595), and 1287 nm for the toluene/methanol, THF/methanol, and chloroform/methanol dispersions, respetively. These $D_h$ values were much larger than those lamella sizes obtained from the TEM imaging results (50 ~ 120 nm, Fig. S20). This picture was again due to the presence of the 10 vol % nonselective solvents of toluene, THF, or chloroform in the dispersions,[53,S4−S6] consistent with the

above larger-sized aggregates *via* vesicles formed by **SEW-3−5** in the chloroform/methanol mixture solvent (v/v = 1/9).

**The hierarchical self-assembly of miktoarm star copolymers showed pathway complexity.** As already addressed in many cases, both block copolymers[1,4,10−12,24,25,36−39] and miktoarm stars[46,47,50,51] cannot be directly dissolved in selective solvents as a result of long insoluble blocks. Therefore, the copolymers were first dispersed in a common good solvent for all the blocks. Successive addition of a nonsolvent led to a worsened solvent quality for one block, driving the copolymers to aggregate into micellelike nano-objects. The final dispersions were colloidally stable and no precipitated copolymers are observed over time. In all of those cases, the copolymers were popularly considered to exist as forms of single chains or single stars in nonselective solvents.

Here, starting with a POM cluster of $K_4[SiW_{12}O_{40}]$ and block copolymers of $\mathbf{PS}_{\boldsymbol{n}}\text{-}\boldsymbol{b}^{+}\text{-}\mathbf{PEG}_{\boldsymbol{m}}\mathbf{I}^{-}$ ($\boldsymbol{n}$ = 17, 26, 39, 57, 81; $\boldsymbol{m}$ = 45), where the miktoarm stars of **SEW-1−5** formed then,[53] we fabricated a series of hierarchical assemblies with multiple levels of structural complexity (Fig. 7). **SEW-3−5** self-assembled in the chloroform/methanol mixture solvents to form normal vesicles with a $\mathbf{PS}_{\boldsymbol{n}}$ core ($\boldsymbol{n}$ = 39, 57, 81) and a $[\alpha\text{-}SiW_{12}O_{40}]^{4-}/\mathbf{PEG_{45}}$ corona (Fig. 5, 6, and S10−S12). This scenario coincided well with the changes of the solvent quality, where the mixture solvents were poor and good for the $\mathbf{PS}_{\boldsymbol{n}}$ arm and $[\alpha\text{-}SiW_{12}O_{40}]^{4-}/\mathbf{PEG_{45}}$ block, respectively. Consequently, both the original reverse cylindrical and ricelike/spherical micelles of **SEW-3−5** in chloroform[53] experienced molecular reorganizations to create the normal vesicles in the present chloroform/methanol mixture solvents. The difference was that such molecular reorganizations were not necessary in the case of **SEW-1**, where nano-sized lamellae were obtained in those methanol based mixture solvents with a percentage of 90 vol % (Fig. S20). This was definitely attributed to the formation of nanometric bilayered structures of **SEW-1** with a $\mathbf{PS_{17}}$ core and $[\alpha\text{-}SiW_{12}O_{40}]^{4-}/\mathbf{PEG_{45}}$ corona in toluene, THF, or chloroform. Such core−corona structures were compatible with the successive addition of 90 vol % methanol. Before the formation of these normal vesicles and lamellae with colloidal stability, the micelle-structured procursors existed in those nonselective solvents. Such micelle-intermediate pictures were never demonstrated and stood in clear conflict with those common single molecule considerations of block copolymers or miktoarm stars in nonselective solvents.

**SEW-2** self-assembled into bundlelike fibers and sheetlike assemblies in the THF/methanol (Fig. 2) and toluene/methanol mixture solvents, respectively (Fig. 3). The original cylindrical micelles[53] formed in THF and toluene still maintained their core−corona micelle structures, where the outside coronas were the $\mathbf{PS_{26}}$ chains and the cores were the $[\alpha\text{-}SiW_{12}O_{40}]^{4-}/\mathbf{PEG_{45}}$ composites. No molecular reorganizations emerged as a result of the variations of the solvent quality. Moreover, the dispersions were colloidally instable and the surfaces of the casting films were hydrophobic. These were in contrast to the generation of the normal vesicles when **SEW-3−5** were dispersed in the chloroform/methanol mixture solvents, where the miktoarm star copolymers were reorganized correspondingly. Combining the present experimental insights together with the previous theoretical considerations,[59,60] we inferred that the driving forces for these bundles and sheets were assigned to inter-cylinder van der Waals attractions, as demonstrated by the full interpenetration of the $\mathbf{PS_{26}}$ chains between the cylindrical cores. In addition, the $\mathbf{PS_{26}}$ chains in both the outside and inside coronas were highly stretched as a result of the contractive cylindrical cores (Table 2 and S4). The sheetlike assemblies of **SEW-3−5** were generally formed in the toluene/methanol mixture solvent (v/v = 1/1, Fig. S5−S7). The original ricelike or spherical micelles were found to evolve into cylindrical micelles, which further *in situ* formed the free-standing sheets through inter-cylinder van

der Waals attractions. These contrasted sharply with the cylinder-to-sphere fragmentation found in both the chloroform/methanol (Fig. S8 and S16) and THF/methanol mixture solvents (Fig. S17 and S18). This difference was likely due to the presence of π–π interactions between the $\mathbf{PS}_{n}$ arms ($\boldsymbol{n}$ = 26, 39, 57, 81) and toluene molecules under the worsened solvent quality conditions. Further increasing the methanol to 75 vol % and 90 vol % allowed us to fabricate nano-sized hollow spheres of **SEW-5**, in which the spherical micelles of **SEW-5** were held unexpectedly with a $[\alpha\text{-}SiW_{12}O_{40}]^{4-}$/$\mathbf{PEG_{45}}$ core and a $\mathbf{PS_{81}}$ corona (Fig. S5 and S6). The driving force was due to the inter-sphere van der Waals attractions. Such van der Waals attractions also occurred between the outside coronas of the hollow spheres, which further caused the precipitated solutions and thus colloidal instability. Clearly, the aforementioned van der Waals attractions were cooperatively anisotropic for the construction of the nonclassical aggregates such as bundle- and sheetlike assemblies and hollow spheres. The difference was that the solid multi-micelle spheres of the miktoarm stars were captured in the THF/methanol (**SEW-3−5**, Fig. S16−S18) or chloroform/methanol mixture solvents (**SEW-2**, Fig. S8) as a result of isotropic van der Waals attractions between the spherical micelles.

**We cannot exclude the possibility that the POM interface stabilize the core or prevent the core from swelling/disassembly.** When one considered the aforementioned molecular reorganization to generate regular vesicles in the chloroform/methanol mixture solvents, such stabilizing or preventing contribution was not dominant.

**Additional References:**


S1 (*a*) G. S. Grest, *Macromolecules*, 1994, **27**, 3493; (*b*) S. Huissmann, R. Blaak and C. N. Likos, *Macromolecules*, 2009, **42**, 2806; (*c*) F. LoVerso, S. A. Egorov and K. Binder, *Macromolecules*, 2012, **45**, 8892.

S2 (*a*) M. Kapnistos, D. Vlassopoulos, G. Fytas, K. Mortensen, G. Fleischer and J. Roovers, *Phys. Rev. Lett.*, 1998, **85**, 4072; (*b*) E. Stiakakis, D. Vlassopoulos, B. Loppinet, J. Roovers and G. Meier, *Phys. Rev. E*, 2002, **66**, 051804; (*c*) D. Vlassopoulos, *J. Polym. Sci. Part B: Polym. Phys.*, 2004, **42**, 2931.

S3 N. Kimizuka, T. Kawasaki, K. Hirata and T. Kunitake, *J. Am. Chem. Soc.*, 1998, **120***,* 4094.

S4 M. Gauthier, L. Tichagwa, J. S. Downey and S. Gao, *Macromolecules*, 1996, **29***,* 519.

S5 D. Taton, E. Cloutet and Y.Gnanou, *Macromol. Chem. Phys.*, 1998, **199***,* 2501.

S6 C. Tsitsilianist, D. Papanagopoulos and P. Lutz, *Polymer* 1995, **36**, 3745.


**Table S1** Solubility parameters ($J^{1/2}/cm^{3/2}$) of toluene, methanol, toluene/methanol mixture solvents, and polymers and deviations between the solubility parameters of toluene/methanol mixture solvents and polymers

| $V_{s1}$ / vol % | $V_{s4,1}$ / vol % | $\delta_1$ | $\delta_4$ | $\delta_{mix}$ | $\delta_{PS}$ | $\delta_{PEG}$ | $\Delta = \lvert\delta_{mix}-\delta_{PEG}\rvert$ | $\Delta = \lvert\delta_{mix}-\delta_{PS}\rvert$ |
|---|---|---|---|---|---|---|---|---|
| 100 | 0 | 18.2 | 29.7 | 18.20 | 18.6 | 20.2 | 2.00 | 0.40 |
| 90 | 10 | 18.2 | 29.7 | 19.35 | 18.6 | 20.2 | 0.85 | 0.75 |
| 85 | 15 | 18.2 | 29.7 | 19.92 | 18.6 | 20.2 | 0.28 | 1.32 |
| 75 | 25 | 18.2 | 29.7 | 21.08 | 18.6 | 20.2 | 0.88 | 2.48 |
| 50 | 50 | 18.2 | 29.7 | 23.95 | 18.6 | 20.2 | 3.75 | 5.35 |
| 25 | 75 | 18.2 | 29.7 | 26.83 | 18.6 | 20.2 | 6.63 | 8.23 |
| 10 | 90 | 18.2 | 29.7 | 28.55 | 18.6 | 20.2 | 8.35 | 9.95 |
| 0 | 100 | 18.2 | 29.7 | 29.70 | 18.6 | 20.2 | 9.50 | 11.10 |

**Table S2** Solubility parameters ($J^{1/2}/cm^{3/2}$) of chloroform, methanol, chloroform/methanol mixture solvents, and polymers and deviations between the solubility parameters of chloroform/methanol mixture solvents and polymers

| $V_{s2}$ / vol % | $V_{s4,2}$ / vol % | $\delta_2$ | $\delta_4$ | $\delta_{mix}$ | $\delta_{PS}$ | $\delta_{PEG}$ | $\Delta = \lvert\delta_{mix}-\delta_{PEG}\rvert$ | $\Delta = \lvert\delta_{mix}-\delta_{PS}\rvert$ |
|---|---|---|---|---|---|---|---|---|
| 100 | 0 | 19.0 | 29.7 | 19.00 | 18.6 | 20.2 | 1.20 | 0.40 |
| 90 | 10 | 19.0 | 29.7 | 20.07 | 18.6 | 20.2 | 0.13 | 1.47 |
| 85 | 15 | 19.0 | 29.7 | 20.60 | 18.6 | 20.2 | 0.40 | 2.00 |
| 75 | 25 | 19.0 | 29.7 | 21.68 | 18.6 | 20.2 | 1.48 | 3.08 |
| 50 | 50 | 19.0 | 29.7 | 24.35 | 18.6 | 20.2 | 4.15 | 5.75 |
| 25 | 75 | 19.0 | 29.7 | 27.02 | 18.6 | 20.2 | 6.82 | 8.42 |
| 10 | 90 | 19.0 | 29.7 | 28.63 | 18.6 | 20.2 | 8.43 | 10.03 |
| 0 | 100 | 19.0 | 29.7 | 29.70 | 18.6 | 20.2 | 9.50 | 11.10 |

**Table S3** Solubility parameters ($J^{1/2}/cm^{3/2}$) of THF, methanol, THF/methanol mixture solvents, and polymers and deviations between the solubility parameters of THF/methanol mixture solvents and polymers

| $V_{s3}$ / vol % | $V_{s4,3}$ / vol % | $\delta_3$ | $\delta_4$ | $\delta_{mix}$ | $\delta_{PS}$ | $\delta_{PEG}$ | $\Delta = \lvert\delta_{mix}-\delta_{PEG}\rvert$ | $\Delta = \lvert\delta_{mix}-\delta_{PS}\rvert$ |
|---|---|---|---|---|---|---|---|---|
| 100 | 0 | 18.8 | 29.7 | 18.80 | 18.6 | 20.2 | 1.40 | 0.20 |
| 90 | 10 | 18.8 | 29.7 | 19.89 | 18.6 | 20.2 | 0.31 | 1.29 |
| 85 | 15 | 18.8 | 29.7 | 20.44 | 18.6 | 20.2 | 0.24 | 1.84 |
| 75 | 25 | 18.8 | 29.7 | 21.52 | 18.6 | 20.2 | 1.33 | 2.93 |
| 50 | 50 | 18.8 | 29.7 | 24.25 | 18.6 | 20.2 | 4.05 | 5.65 |
| 25 | 75 | 18.8 | 29.7 | 26.98 | 18.6 | 20.2 | 6.78 | 8.38 |
| 10 | 90 | 18.8 | 29.7 | 28.61 | 18.6 | 20.2 | 8.41 | 10.01 |
| 0 | 100 | 18.8 | 29.7 | 29.70 | 18.6 | 20.2 | 9.50 | 11.10 |

$V_{s1}$: Toluene volume ratios in the toluene/methanol mixtures. $V_{s2}$: Chloroform volume ratios in the chloroform /methanol mixtures. $V_{s3}$: THF volume ratios in the THF/methanol mixtures. $V_{s4,1}$: Methanol volume ratios in the toluene/methanol mixtures. $V_{s4,2}$: Methanol volume ratios in the chloroform /methanol mixtures. $V_{s4,3}$: Methanol volume ratios in the THF/methanol mixtures. $\delta_1$: Solubility parameter of toluene. $\delta_2$: Solubility parameter of chloroform. $\delta_3$: Solubility parameter of THF. $\delta_4$: Solubility parameter of methanol. $\delta_{mix}$: Solubility parameters of the toluene/methanol mixtures. $\delta_{PS}$: Solubility parameter of poly(styrene). $\delta_{PEG}$: Solubility parameter of Poly(ethylene glycol) methyl ether.

**Table S4** Packing parameters of sheetlike assemblies formed by **SEW-2−5** in the toluene/methanol mixture solvent with a methanol percentage of 50 Vol %

| | **SEW-2** | **SEW-3** | **SEW-4** | **SEW-5** |
|---|---|---|---|---|
| $D_{CD}$ (nm)[a] | 6.0 | 5.6 | 4.8 | 4.2 |
| $D_{DM}$ (nm)[b] | 8.3 | 9.5 | 10.9 | 13.1 |
| $T_S$ (nm)[c] | 14.3 | 15.1 | 15.7 | 17.3 |
| $\sigma$ (chains/nm$^2$)[d] | 0.54 | 0.57 | 0.68 | 0.76 |
| $L_C$ (nm)[e] | 6.5 | 9.75 | 14.25 | 20.25 |

[a]Core diameter of cylindrical micelles. [b]Distance between the cylindrical cores in the sheetlike assemblies. [c]Thickness of the sheetlike assemblies. [d]Grafting density of the $\mathbf{PS}_{\boldsymbol{n}}$ chains ($\boldsymbol{n}$ = 26, 39, 57, 81). [e]Contour length of the $\mathbf{PS}_{\boldsymbol{n}}$ chains.

**Table S5** Packing parameters of cylindrical micelles, bundled fibers, and multi-micelle aggregates formed by **SEW-2** in the methanol based mixture solvents

| Common Solvent | Volume Ratio of Methanol | $D_{CD}$ (nm)[a] | $D_{CT}$ (nm)[b] | $\sigma$ (chains/nm$^2$)[c] | $D_{DM}$ (nm)[d] |
|---|---|---|---|---|---|
| THF | 0 [e] | 6.3 (c) | 4.6 | 0.51 | - |
| | 50% | 5.0 (c) | 6.7 | 0.64 | 5.6 |
| | 90% | 4.8 (c) | 6.5 | 0.67 | 5.4 |
| chloroform | 50% | 4.8 (c) | 6.3 | 0.67 | 5.4 |
| | | 6.5 (s) | 6.0 | 0.35 | 4.8 |
| | 90% | 4.5 (c) | 5.9 | 0.71 | 5.9 |
| | | 4.8 (s) | 5.2 | 0.64 | 4.5 |
| toluene | 0 [e] | 6.3 (c) | 4.6 | 0.51 | - |
| | 90% | 4.8 (c) | 6.0 | 0.67 | 4.2 |

[a]Core diameter of cylindrical (c) or spherical micelles (s). [b]Corona thickness. [c]Grafting density of the $\mathbf{PS_{26}}$ chain. [d]Distance between the micellar cores in the bundlelike fibers or solid spheres. [e]Data from our previous work.[53] The contour length of the $\mathbf{PS_{26}}$ chain was (0.25 × 26 = 6.5 nm).

**Table S6** Packing parameters of hollow nanostructures formed by **SEW-3** and **SEW-5** in the toluene/methanol mixture solvent with a methanol composition of 75 vol %

| Sample | Volume Ratio of Methanol | $D_{AD}$ (nm) [a] | $D_{CT}$ (nm) [b] | $D_{CD}$ (nm) [c] | $D_{DM}$ (nm) [d] | $D_{RM}$ (nm) [e] | $\sigma$ (chains/nm$^2$) [f] | $N_{agg}$ |
|---|---|---|---|---|---|---|---|---|
| **SEW-5** | 0 | - | 4.9 | 8.8 | - | 18.6 | 0.48 | 29 [g] |
| | 75% | 160 | 9.6 | 6.2 | 9.0 | 25.4 | 0.33 | 10 [g]<br>286 [f]<br>2860 [g] |
| **SEW-3** | 75% | 130 | 7.5 | 4.7 | 6.5 | 19.4 | 0.26 | 4.5 [g]<br>355 [f]<br>7632 [g] |

[a]Average diameter of hollow nanostructures. [b]Corona thickness of the $\mathbf{PS}_n$ chains ($\boldsymbol{n}$ = 39, 81) in the hollow nanostructures. [c]Core diameter of reverse micelles. [d]Distance between the micellar cores in the hollow nanostructures. [e]Total diameter of reverse micelles. [f]Grafting density of the $\mathbf{PS}_n$ chains. [g]Estimated by dividing the volume of the micelle core by the hydrophilic volume per formula of the miktoarm stars (See Fig. 1). [h]Estimated by dividing the surface area of the hollow nanostructure at the central location of the micelle unit. [i]Aggregation number of the miktoarm stars in the hollow nanostructures estimated with $N_{agg}$ [g] and $N_{agg}$ [h].

**Table S7** Packing parameters of regular lamellae and vesicles formed by **SEW-1** and **SEW-3−5** in the chloroform/methanol mixture solvents.

| | **SEW-1** | **SEW-3** | **SEW-4** | **SEW-5** |
|---|---|---|---|---|
| $D_{CD}$ (nm)[a] | 2.6 | 11.2 | 12.7 | 14.8 |
| $A_0$ (nm$^2$)[b] | 2.15 | 1.15 | 1.48 | 1.80 |

[a]Core diameter of regular vesicles for the $\mathbf{PS}_n$ chains ($n$ = 17, 39, 57, 81). [b]Interfacial area per chain for the $\mathbf{PS}_n$ arms.

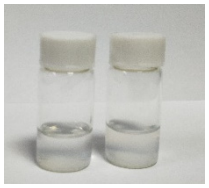

**Fig. S1 SEW-2** formed precipitates in the THF/methanol mixture solvents with methanol contents of 50 vol % (left) and 90 vol % (right) at the bottom of the vials.

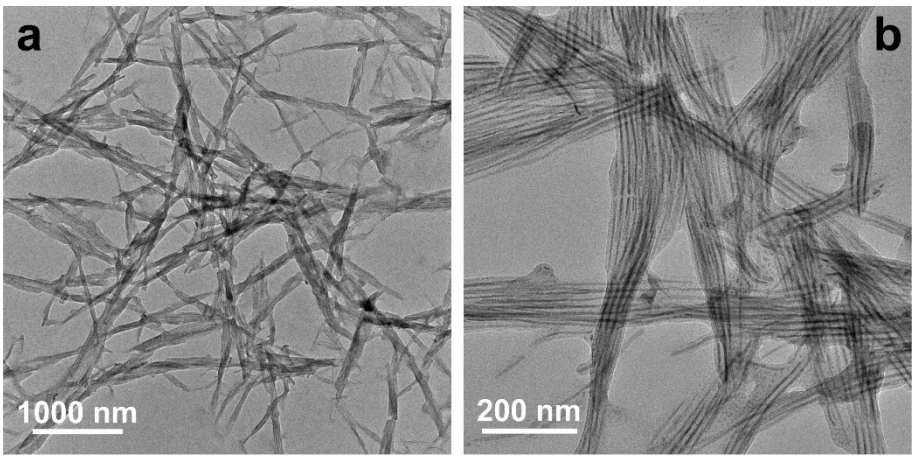


**Fig. S2** BF-TEM demonstrated that **SEW-2** self-assembled to form bundled fibers in the THF/methanol mixture with a methanol percentage of 90 vol %.

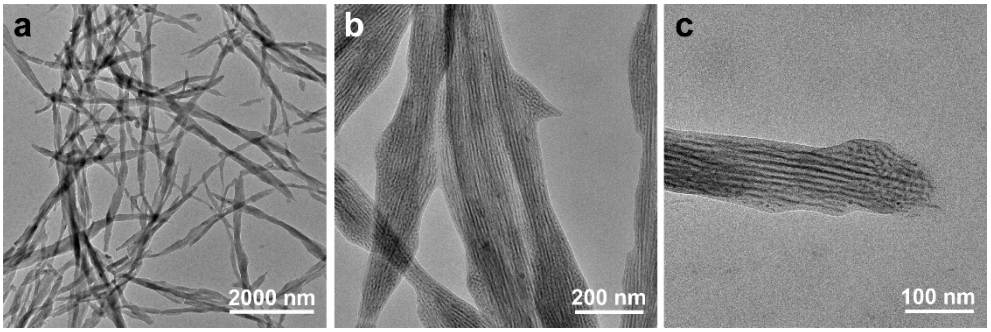


**Fig. S3** BF-TEM demonstrated that **SEW-2** self-assembled to form bundled fibers in the toluene/methanol mixture with a methanol percentage of 90 vol %.

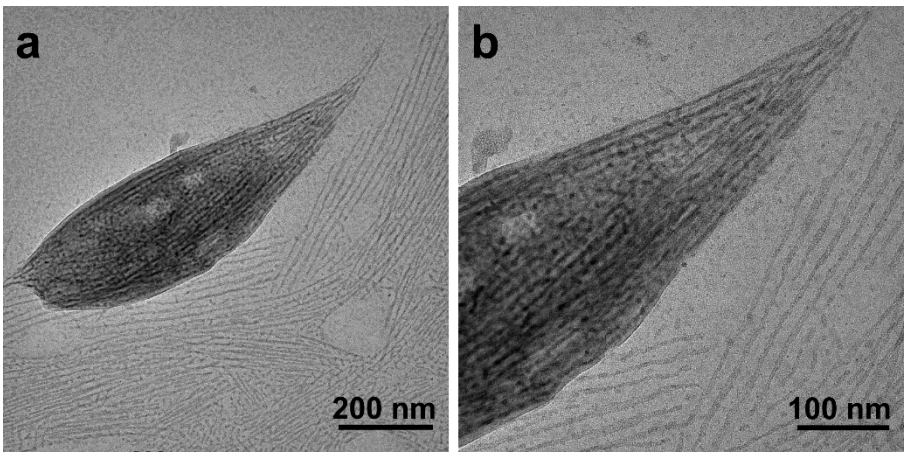


**Fig. S4** when **SEW-2** was dispersed in the toluene/methanol mixture solvent with an intermediate methanol content of 75 vol %, the resulting TEM images showed a coexistence of free-standing sheets and bundled nanofibers.

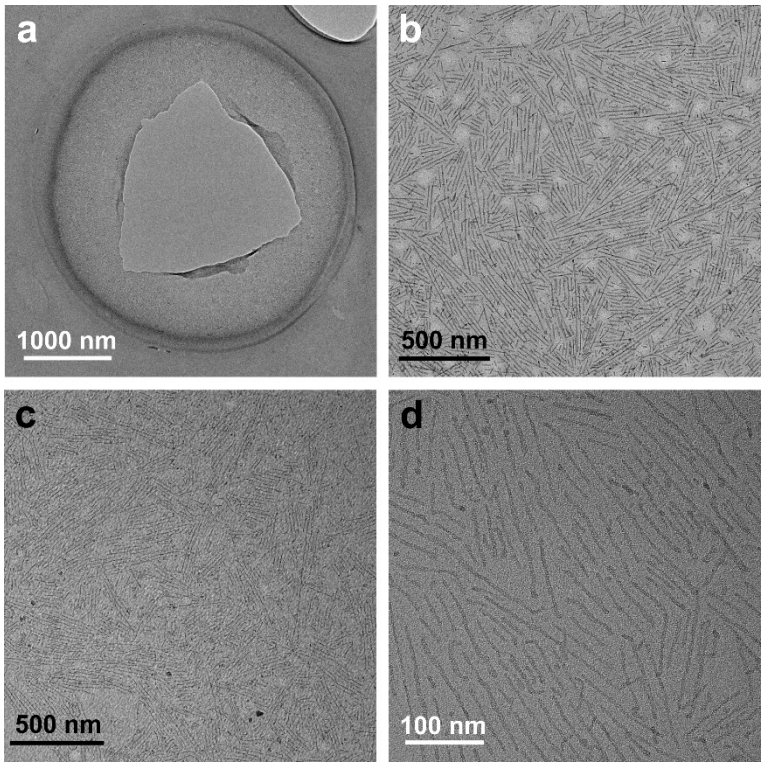


**Fig. S5** The miktoarm stars of **SEW-3** (a and b) and **SEW-4** (c and d) self-assembled to generate sheetlike assemblies in the toluene/methanol mixture solvent with a methanol content of 50 vol % (0.5 mg/mL).

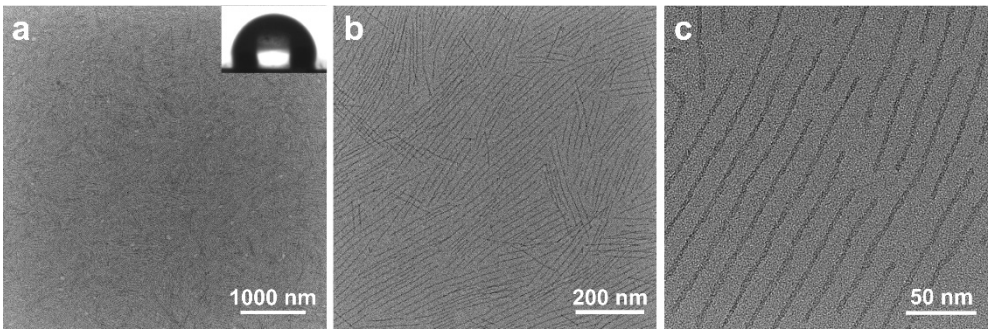


**Fig. S6** As revealed in the BF-TEM images (a, b, and c), **SEW-5** self-assembled into sheetlike assemblies in the toluene/methanol mixture solvent with a methanol percentage of 50 vol %. The inset (a) was indicative of a water contact angle of 106°. The original spherical micelles formed in toluene were transformed to form cylindrical micelles in the sheetlike assemblies under the present solvent condition.

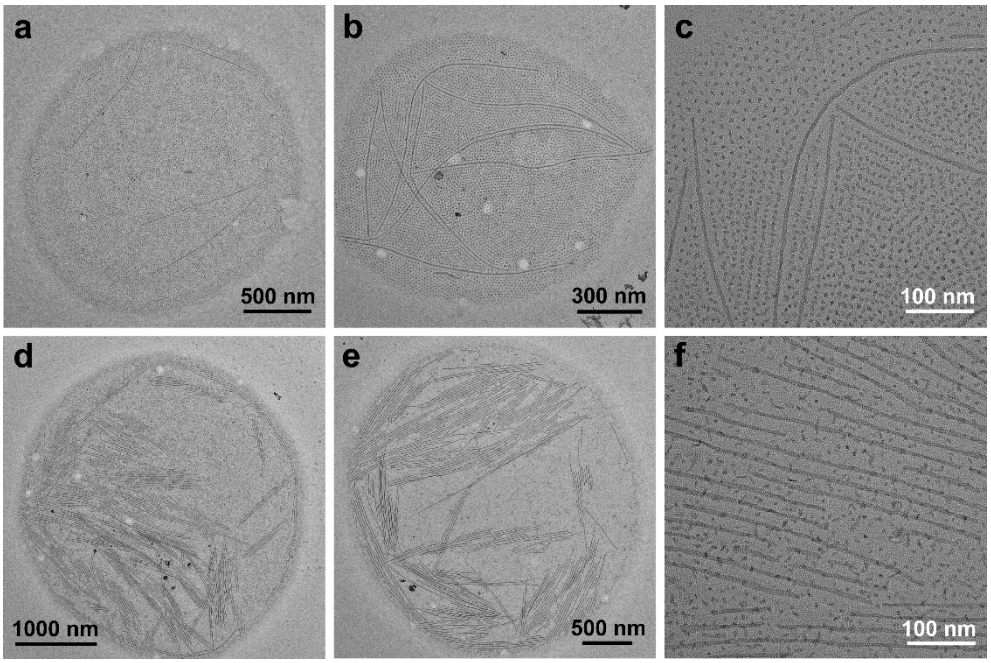


**Fig. S7** BF-TEM images of **SEW-5** were obtained from the toluene/methanol mixture solvents with methanol percentages of 10 vol % (a, b, and c) and 25 vol % (d, e, and f). The TEM results showed that cylindrical micelles coexisted with spherical micelles and the number ratio of the cylinder was increased from 5 % to 30 %, indicative of sphere-to-cylinder intermediate morphologies under these solvent conditions.

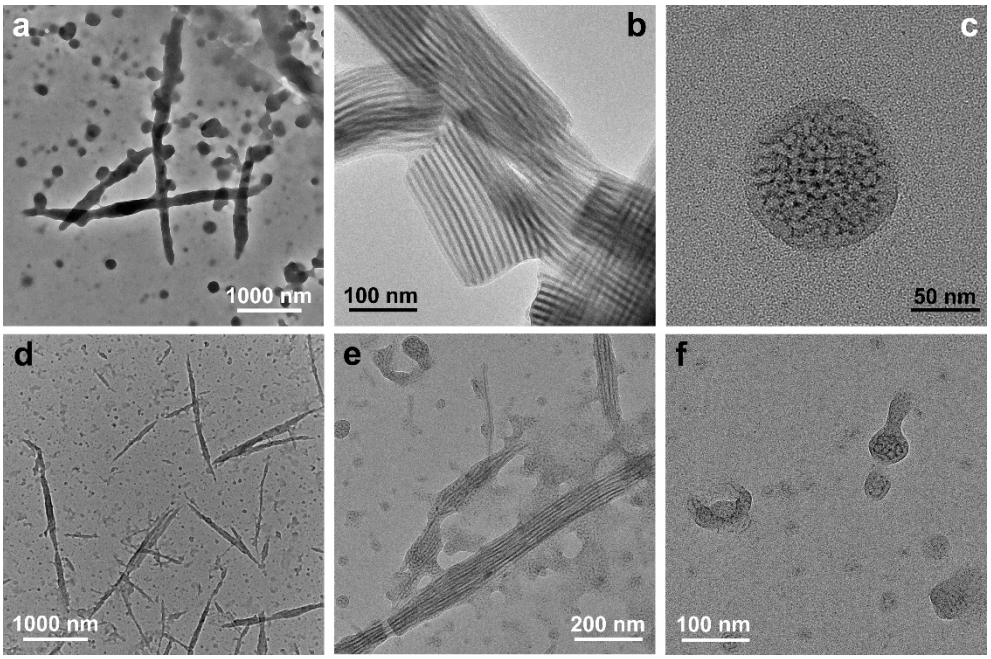


**Fig. S8 SEW-2** self-assembled to form bundlelike nanofibers coexisting with solid spheres on dispersion in the chloroform/methanol mixture solvents with methanol volume ratios of 50 % (a−c) and 90% (d−e).

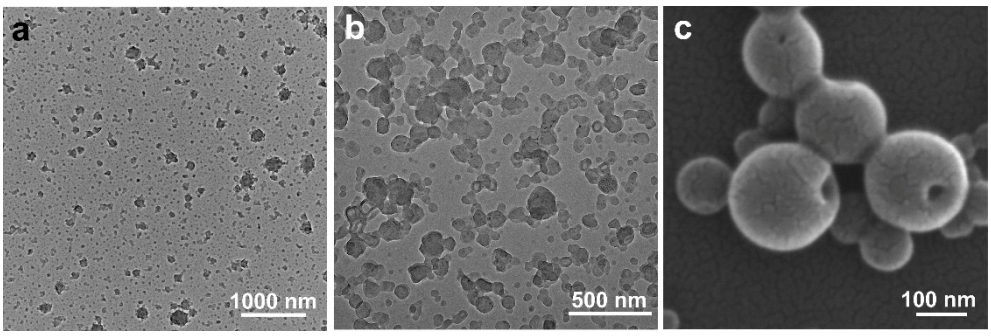


**Fig. S9** BF-TEM (a and b) and SEM images (c) demonstrated that **SEW-5** self-assembled to nano-sized hollow aggregates in the toluene/methanol mixture with a methanol percentage of 90 vol %.

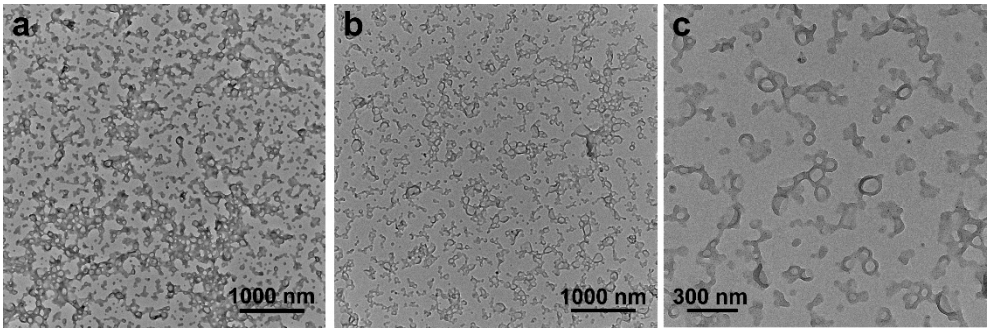


**Fig. S10 SEW-4** self-assembled into normal vesicles in the chloroform/methanol mixture solvents of methanol percentages of 75 vol % (a) and 90 vol % (b and c).

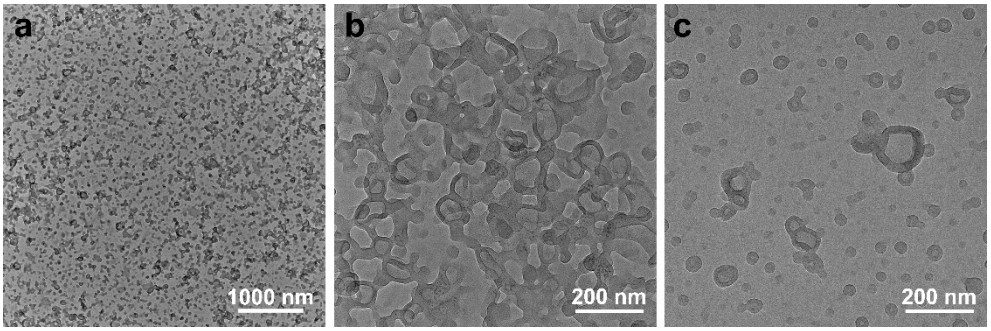


**Fig. S11 SEW-5** self-assembled into normal vesicles in the chloroform/methanol mixture solvents of methanol percentages of 50 vol % (a and b) and 90 vol % (c).

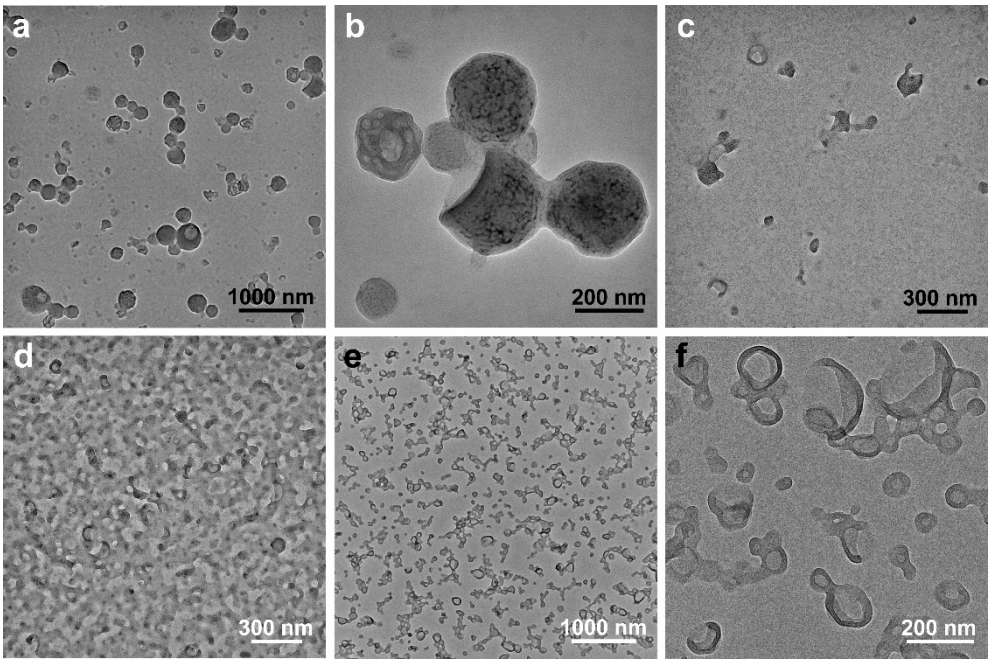


**Fig. S12** The coexistence of regular bilayered vesicles with solid spheres was arrested clearly when **SEW-3** was dispersed in the chloroform/methanol mixture solvents with methanol contents of 25 vol % (a and b), 50 vol % (c), and 75 vol % (d). Only when the methanol content was increased to 90 vol %, the original reverse micelles of **SEW-3** were completely transformed to form regular bilayered vesicles (e and f).

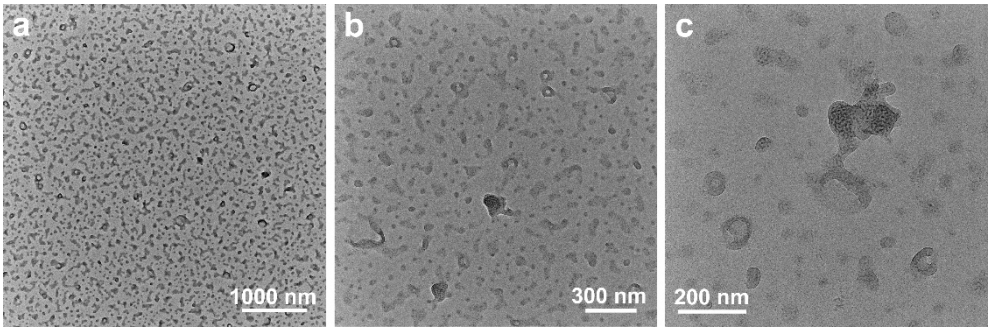


**Fig. S13** The dispersion of **SEW-3** in the toluene/methanol mixture solvent with a methanol volume ratio of 90 % showed morphological existence of hollow nanostructures with normal vesicles (a−c).

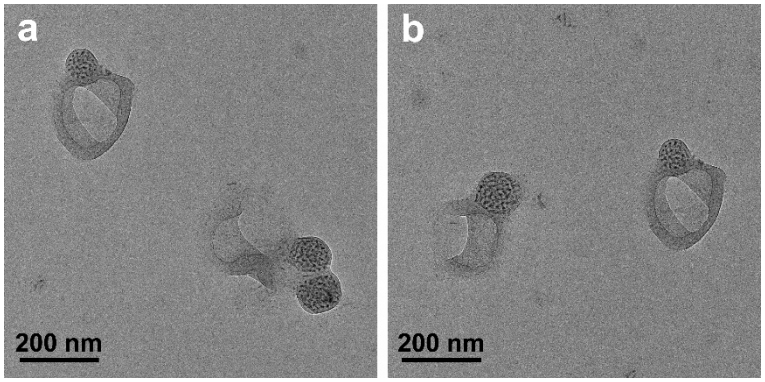


**Fig. S14** The dispersion of **SEW-4** in the toluene/methanol mixture solvent with a methanol volume ratio of 75 % showed morphological existence of hollow nanostructures with normal vesicles (a and b).

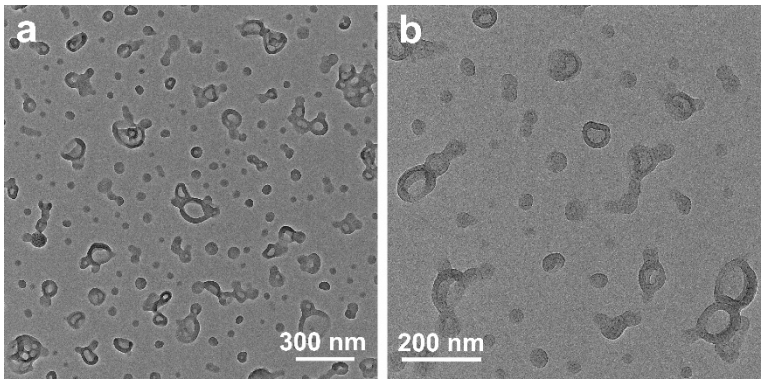


**Fig. S15 SEW-4** self-assembled into a pure vesicle phase in the toluene/methanol mixture solvent with a methanol volume ratio of 90 % (a and b).

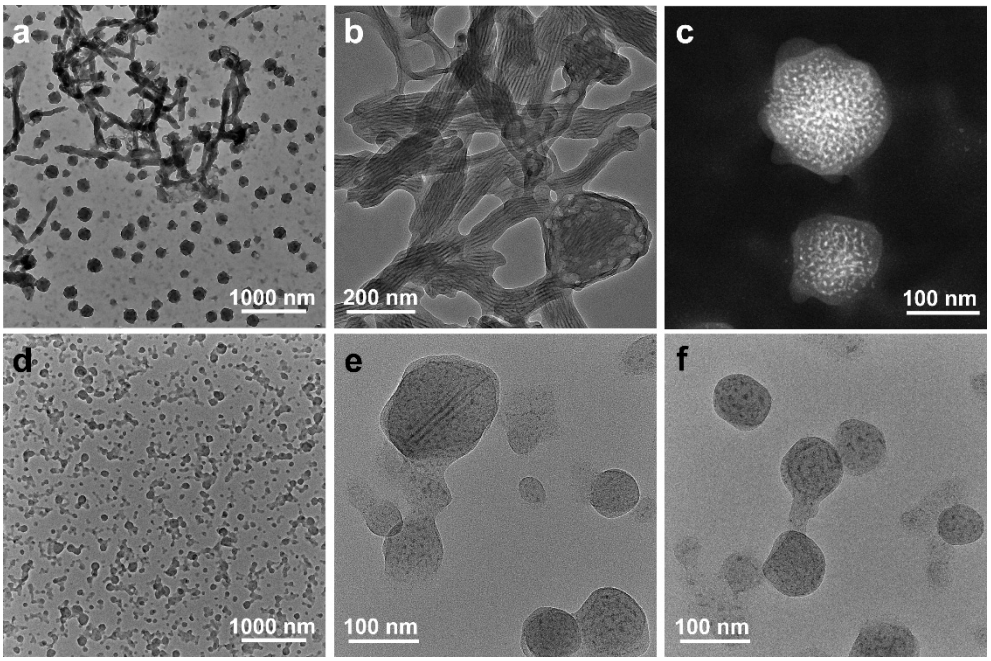


**Fig. S16 SEW-3** self-assembled into multi-micelle aggregates in the THF/methanol mixture solvents with methanol volume ratios of 50 % (a−c) and 90 % (d−f). Cylindrical or rodlike micelles coexisted with spherical micelles.

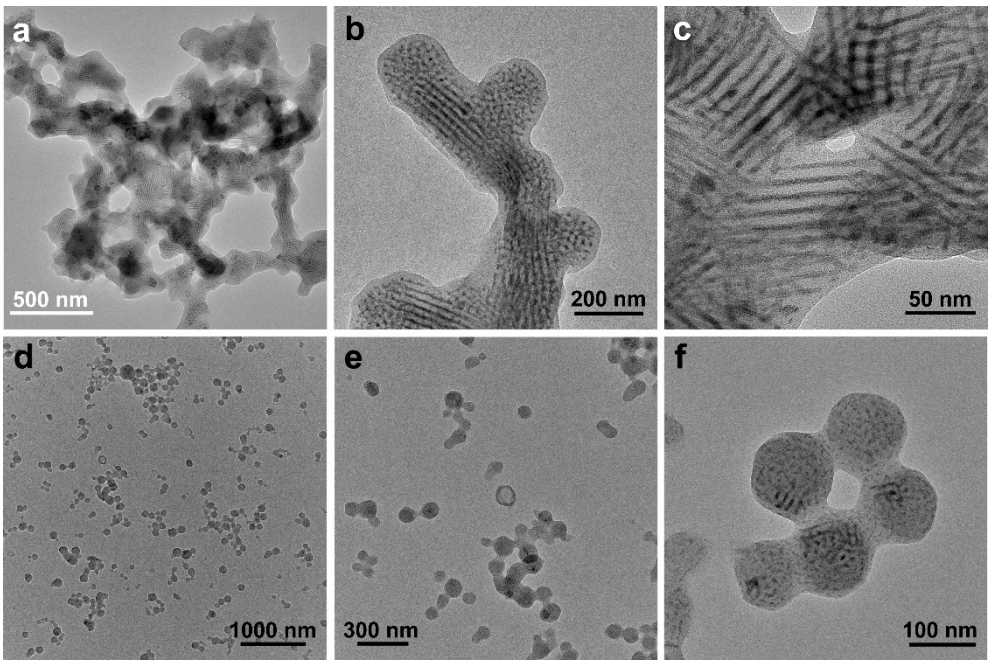


**Fig. S17 SEW-4** self-assembled into multi-micelle aggregates in the THF/methanol mixture solvents with methanol volume ratios of 50 % (a−c) and 90 % (d−f).

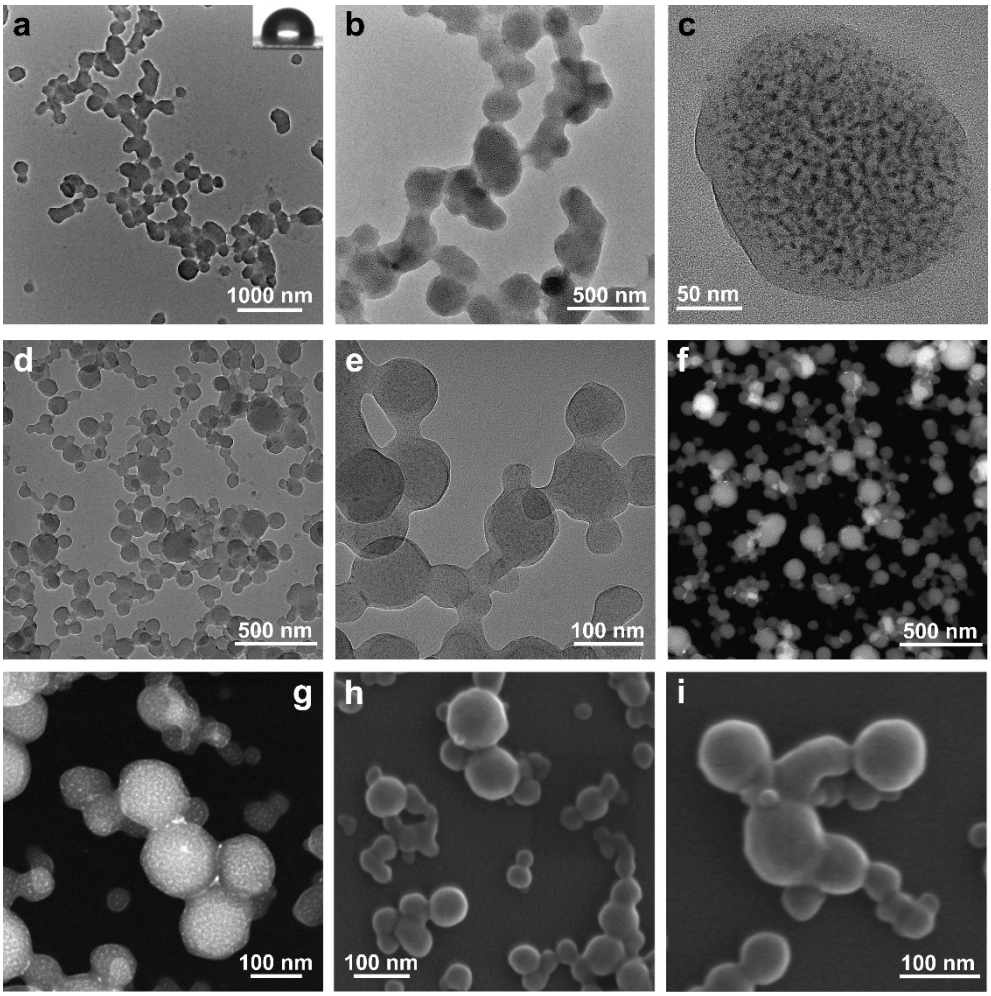


**Fig. S18 SEW-5** self-assembled into multi-micelle aggregates in the THF/methanol mixture solvents with methanol volume ratios of 50 % (a–c, BF-TEM images) and 90 % (d and e, BF-TEM images; f and g, HAADF-STEM images; h and i, SEM images).

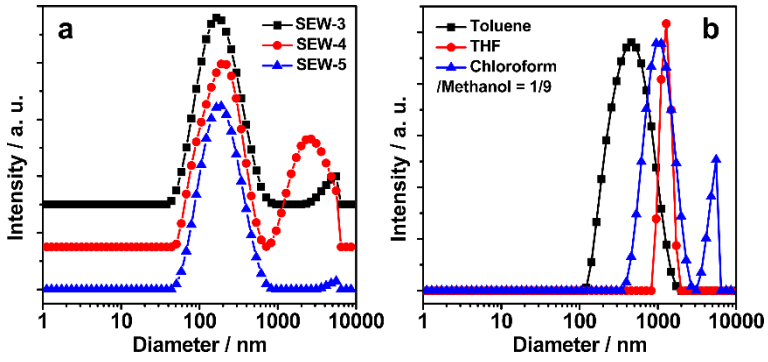


**Fig. S19** DLS plots of **SEW-3–5** (chloroform/methanol = 1/9, a) and **SEW-1** (toluene/methanol, THF/methanol, and chloroform/methanol = 1/9, b).

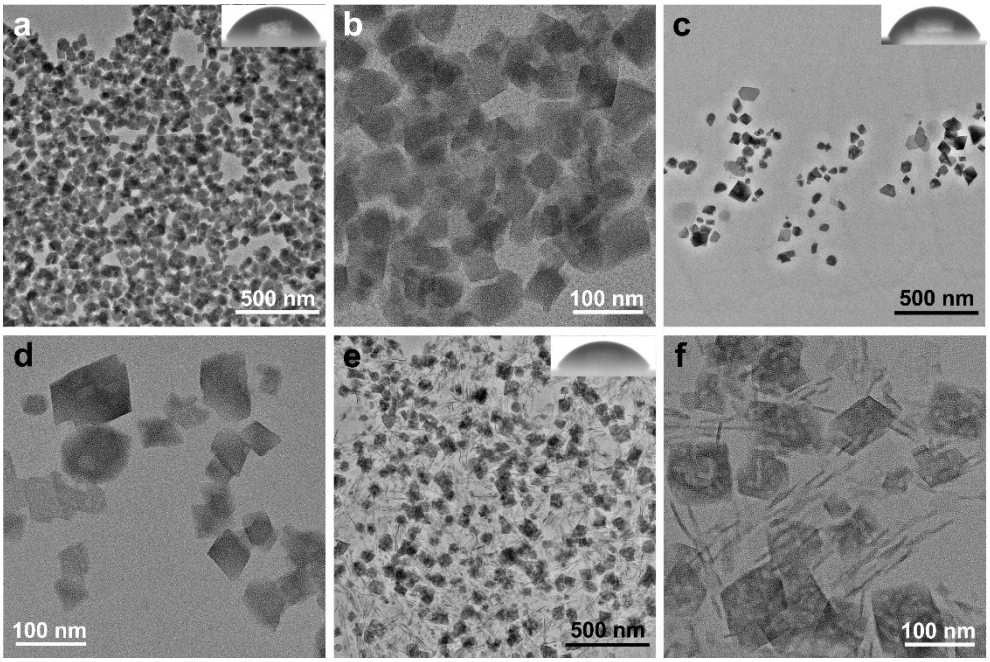


**Fig. S20** SEW-1 self-assemblied to form nano-sized lamellae in the toluene/methanol (a and b), THF/methanol (c and d), andfor chloroform/methanol mixture solvents (e and f). The inset figures (a), (c), and (e) showed a water contact angle of 67°, 66°, and 61°, respectively.